



## Mechanical behavior of segment rebar of shield tunnel in construction stage<sup>\*</sup>

Jun-sheng CHEN<sup>†</sup>, Hai-hong MO

(Department of Civil Engineering, South China University of Technology, Guangzhou 510640, China)

(State Key Laboratory of Subtropical Building Science, South China University of Technology, Guangzhou 510640, China)

<sup>†</sup>E-mail: jschen@scut.edu.cn

Received Oct. 9, 2007; revision accepted Mar. 27, 2008

**Abstract:** In this paper, a 3D finite element (FE) program ADINA was applied to analyzing a tunnel with 9 segment rings. The loads acting on these segment rings included the squeezing action of tail brush of shield machine under attitude deflection, the jacking forces, the grouting pressure and the soil pressure. The analyses focused on the rebar stress in two statuses: (1) normal construction status without shield machine squeezing; (2) squeezing action induced by shield machine under attitude deflection. The analyses indicated that the rebar stress was evidently affected by the construction loads. In different construction status, the rebar stress ranges from -80 MPa to 50 MPa, and the rebar is in elastic status. Even some cracks appear on segments, the stress of segment rebar is still at a low level. It is helpful to incorporate a certain quantity of steel fiber to improve the anti-crack and shock resistance performance.

**Key words:** Shield tunnel, Construction, Segment, Rebar, Finite element (FE) analysis

**doi:** 10.1631/jzus.A0720025

**Document code:** A

**CLC number:** U455

### INTRODUCTION

Segment is the basic structure unit of a shield tunnel. Rebar is the main part of the segment (Fig. 1). The mechanical behavior of the rebar affects the form of reinforcement, the ratio of reinforcement and the cost of whole tunnel. In China, the ratio of reinforcement of finished shield tunnel is 128~165 kg/m<sup>3</sup>. According to Guangzhou Metro, the different ratio of reinforcement causes about 4 million RMB differences in the investment of the shield tunnel (Li and Chen, 2003). Therefore, it is significant to clarify the mechanical behavior of rebar in construction stage, which can save the engineering investment and optimize the segment design.

Foregoing researches (Blom *et al.*, 1999; No-moto *et al.*, 1999; Sramoon and Sugimoto, 2002; Koyama, 2003; Kasper and Meschke, 2004) seldom involve the mechanical behavior of segment rebar. At

present, the methods of research on segment rebar are mostly limited in the indoor full size experiments plus some field measurements. Zhang *et al.* (2002) tested the rebar stress of segment joints through indoor experiments. Chen *et al.* (2004) performed a field measurement on one section of shield tunnel in Guangzhou Metro and researched the property of rebar in different work conditions. Dobashi *et al.* (2004) researched the rational design of steel segmental lining in Central Circular Shinjuku Route. Due to the various types of loads and the complicated boundary conditions, it is very difficult to simulate the actual loads and boundary conditions in indoor experiment. If the loads and boundary conditions are not precisely simulated, the rebar stress measured indoors may have rather large errors. Field measurement may be quite precise for rebar stress. However, for different tunnels, the limited test results cannot reflect the whole picture of their rebar's mechanical behavior under different construction and geological conditions.

<sup>\*</sup> Project supported by Guangzhou Metro of China



Fig.1 Segment reinforcement stacked on the ground

In this paper, a load-structure theory was applied. Based on the research of Zhang *et al.*(2002), Chen *et al.*(2004), and Dobashi *et al.*(2004), a finite element (FE) program of ADINA was adopted to establish a 3D numerical model for the shield tunnel of Guangzhou Metro. In order to simulate the actual situation precisely, the longitudinal bolts, circumferential bolts, longitudinal sealing rod, circumferential sealing rod, key segment and tail of shield machine were considered. The rebar stresses in the normal construction stage and under a squeezing action of shield machine were analyzed.

## CONSTRUCTION STATUS OF SHIELD TUNNEL

### Normal construction status

Normal construction status denotes an ideal status of shield tunnel construction, which means no erection tolerance in segments, a uniform grouting pressure within allowable range, the appropriate jacking forces acting on central line of segment circumferential seam and shield machine attitude with no deviation. Though it is impossible to obtain ideal status, the rebar stress of ideal status is basal value which can be benchmark comparison of other construction status.

### Driving attitude of shield machine with deviation

In the construction stage of a shield tunnel, tolerances between driving route of a shield machine and the design axis are inevitable. It causes the relative position between segment rings and shield machine not be able to maintain in a perfect state, especially during the process of turn and attitude adjustment of the shield machine (Blom *et al.*, 1999; Qin *et al.*, 2004; Li *et al.*, 2006) (Fig.2).

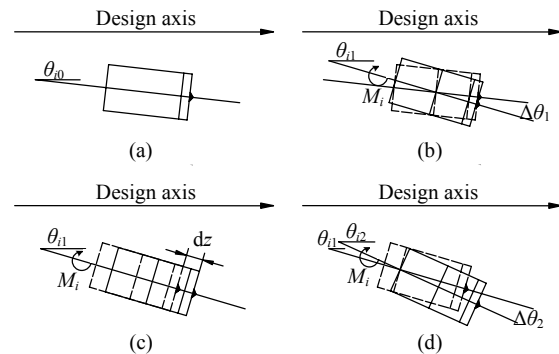


Fig.2 Angle changes between shield machine and design axis. (a) Deviation between design axis and shield machine axis; (b) Shield machine rotates around center of itself; (c) Shield machine drives with deviation between design axis and shield machine axis; (d) The combined situation of (b) and (c)

## PRIMARY LOADS ACTING ON SEGMENTS WHEN SHIELD TUNNEL CONSTRUCTION

### Jacking forces

Jacking force is one of the primary segment loads in the construction stage (Working Group No.2, International Tunneling Association, 2000), which can cause segment cracking, especially when the circular seams of segments are out-of-flatness due to construction and manufacture tolerances. An out-of-flatness of 0.5 mm to 1.0 mm can lead to a huge cleavage moment in next ring. Simultaneously, the eccentric jacking force also causes segment cracking (Li, 2001). If the shield machine axis is not consistent with design axis (Fig.2), the jacking force may become eccentric pressure acting on circular seams obliquely. In Guangzhou Metro, the segment circular seam bears 1600 kN/m pressure along circumferential direction in construction stage (Li, 2001). In present work, jacking forces were simplified to the pressure acting on a circular pad, and the equivalent pressure is 5400 kN/m<sup>2</sup>.

### Grouting pressure

Grouting pressure distribution is complicated. Uneven grouting pressure would cause segment dislocation and even crack. In this paper, it was assumed that the grouting pressure linearly decreased along tunnel axis from Ring 5 (R5) to R7 and finally reached to earth pressure (Zhang *et al.*, 2005) (Fig.3a). According to some results of actual measurement in

Guangzhou and Zhang *et al.*(2005), the grouting pressure is between 0.1 Mpa and 0.5 MPa. In this paper,  $P_{in}$  denotes grouting pressure. In order to reflect general situation,  $P_{in1}$  was assumed to be 0.30 MPa, and  $P_{in2}$  to be 0.45 MPa (Fig.3b).

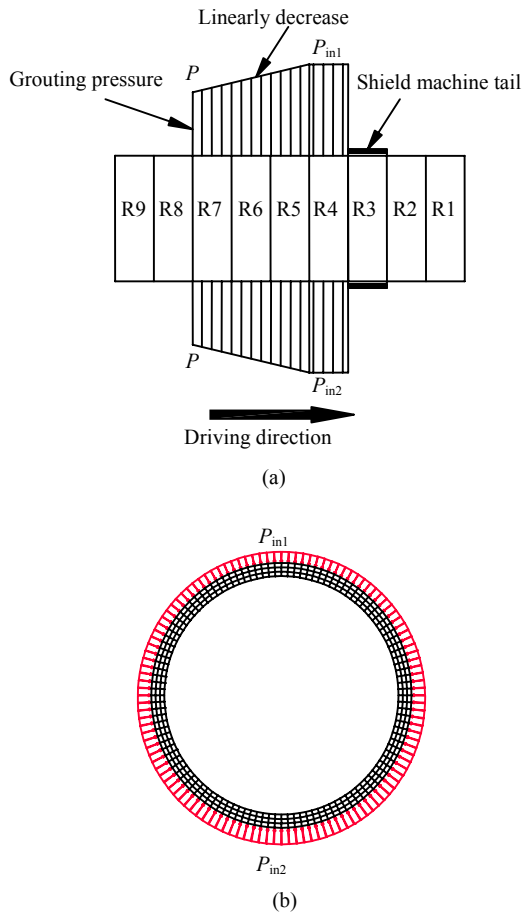


Fig.3 Grouting pressure acting on the segments. (a) Axial distribution; (b) Cross-section distribution

**Earth pressure**

Earth pressure pattern is showed in Fig.4 (Mashimo and Ishimura, 2003). Fig.5 shows the stratum surrounding tunnel structure.

In Fig.4,  $P_1$  is the overlying earth pressure and water pressure acting on the top of segment ring.  $P_2$  is the vertical soil resisting force and vertical water pressure acting on the bottom of segment ring.  $P_3$  is the lateral earth pressure and water pressure acting on the horizontal surface of arch crown.  $P_4$  is the lateral earth pressure and water pressure acting on the horizontal surface of arch bottom.  $P_5$  is the self weight of segments. Resisting forces due to deformation of segment are discussed in subsection “Ground

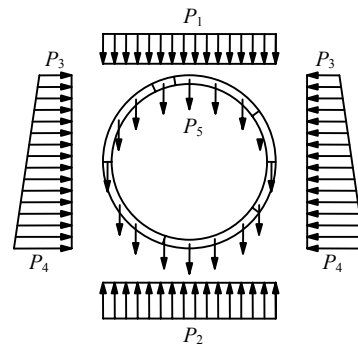


Fig.4 Soil pressure distribution of lining

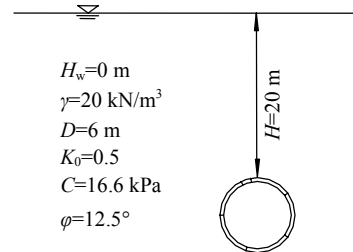


Fig.5 Stratum conditions including depth of shield tunnel and soil parameters

reaction”. Water pressure was not considered separately. The action of water pressure was included in  $P_1$  to  $P_4$ , which is called total stress.

The theory of Terzaghi loosening earth pressure was used to calculate  $P_1$  to  $P_4$  showed in Fig.4 (Terzaghi *et al.*, 1996). The half of loosening range

$$B_1 = R_0 \cot((\pi/4 + \phi/2)/2), \tag{1}$$

where  $R_0$  is the outer radius of segment,  $\phi$  is the internal friction angle of soil. Loosing height of soil

$$h_0 = \frac{B_1(1 - c/(B_1\gamma))}{K_0 \tan \phi} \left(1 - e^{-K_0 \tan \phi \cdot (H/B_1)}\right) + \frac{P_0}{\gamma} e^{-K_0 \tan \phi \cdot (H/B_1)}, \tag{2}$$

where  $K_0$  is the ratio of horizontal earth pressure and vertical earth pressure,  $K_0=0.5$ ,  $c$  is soil cohesion,  $\gamma$  is soil deadweight,  $H$  is overlying soil thickness,  $P_0$  is ground over loads.

Parameters mentioned above were substituted into Eqs.(1) and (2), so  $B_1=6.25$  m and  $h_0=15.37$  m.  $h_0$  is larger than  $2R_0$  which is equal to 12 m. Hence,

$$P_1 = h_0 \gamma = 15.37 \times 20 = 307.40 \text{ kN/m}^2,$$

$$P_2 = P_1 + \pi g = 307.40 + 3.14 \times 7.5 = 330.95 \text{ kN/m}^2,$$

where  $g$  is soil deadweight.

$$P_3 = \lambda P_1 = 153.70 \text{ kN/m}^2,$$

$$P_4 = \lambda(P_1 + \gamma R_0) = 213.70 \text{ kN/m}^2,$$

where  $\lambda$  is lateral coefficient of earth pressure. According to Terzaghi *et al.* (1996),  $\lambda = 0.50$ .

**Ground reaction**

In traditional load-structure theory, the ground reaction is assumed to have a value that corresponds to tunnel deformation and displacement and modeled as ground springs located along the whole periphery of the tunnel (Koyama, 2003; Mashimo and Ishimura, 2003) (Fig.6).

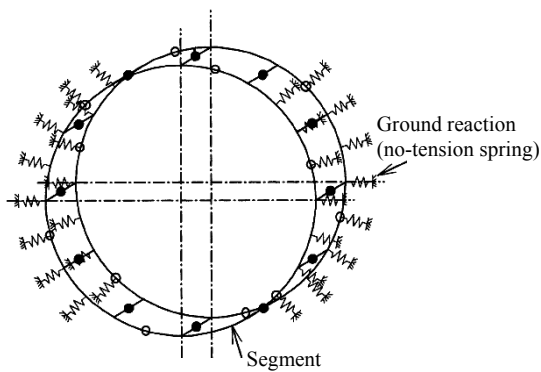


**Fig.6 Spring in traditional load-structure model**

In this paper, a solid mass surrounding tunnel structure was employed to simulate the ground reaction. Between soil and linings a hydrating grout material exists. It is very difficult to ascertain the stiffness of the hydrating grout material. Simultaneously, the thickness of this hydrating grout material is relatively thin and unclear. So, the hydrating grout material was not considered when simulating the interaction between tunnel linings and soil. Grouting pressure mentioned in subsection ‘‘Grouting pressure’’ was adopted to account for actions acted by hydrating grout material (Fig.3).

Contact surfaces were set between inner surfaces of solid mass and segment exterior surfaces (Fig.7). When the tunnel structure deforms under the earth pressure, the contact interaction between the solid mass and segments can restrict the tunnel deformation. Contact forces, including normal force and slid-

ing-frictional force, are automatically computed by ADINA program through iterative process. Therefore, solid mass with contact surfaces can substitute radial ground reaction spring and tangential ground reaction spring which are in traditional load-structure model. The spring stiffness of traditional model is substituted by Young’s modulus of solid mass, and Young’s modulus changes with different soil stratum. Since the first three segment rings are still in shield machine before shield machine drivers forward, the solid mass just surrounds last six segments of the tunnel (Fig.7b). The friction coefficient of soil and segment is set to be 0.3. The solid mass was used only to simulate the ground reaction, so the deadweight of the solid mass was neglected.

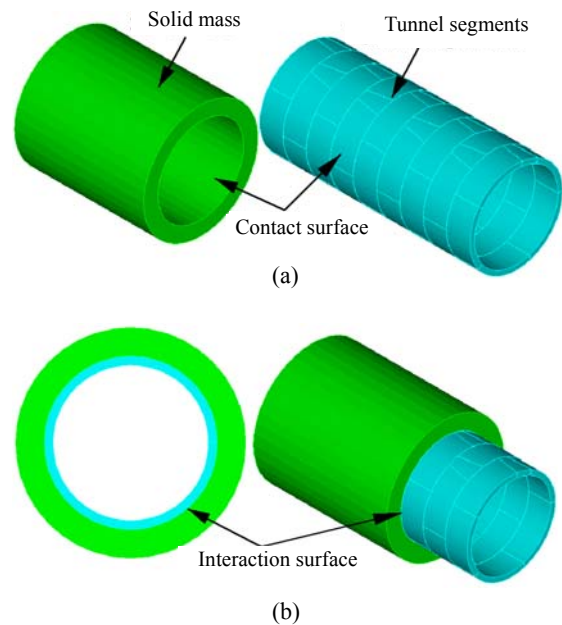


**Fig.7 Contact surfaces between solid mass and tunnel segments. (a) Decomposition map of contact surfaces; (b) Front view of contact surfaces**

**Squeezing action induced by shield machine**

Tail brush showed in Fig.8 is composed of steel wire. The stiffness of new tail brush is small, and the tail brush does not apparently extrude segments. After many times of driving and injecting, the voids of tail brush fill with grouting material. After grouting material hardens, the stiffness of tail brush apparently increases. The squeezing action of tail brush becomes larger and larger. When the shield machine adjusts its attitude, turns or drives with deflection, the space between exterior surface of segments and tail brush

could not be enough. If the attitude adjustment does not match the curved figure of segment, or the deflection angle is too large, the tail brushes and shield shell would extrude the exterior surfaces of segments (Zhu and Ju, 2003) (Figs.9 and 10).

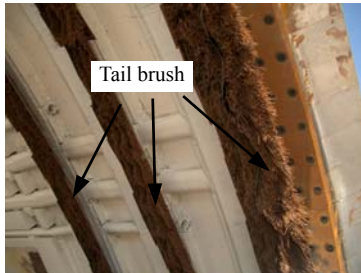


Fig.8 Tail brush of shield machine

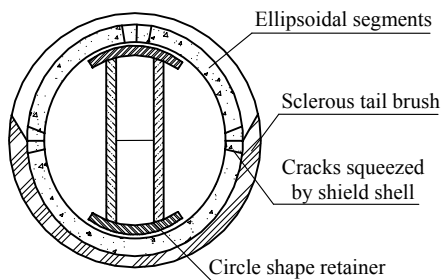


Fig.9 Interaction between segments and equipments of shield machine end part

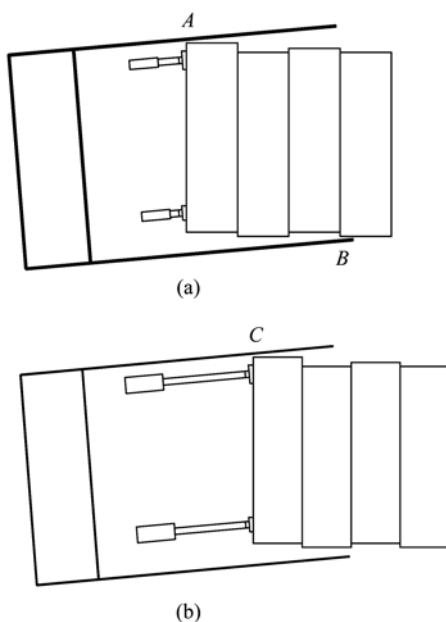


Fig.10 Squeezing action on segments in process of driving forward. (a) Extreme condition 1; (b) Extreme condition 2

The motion attitude of a shield machine has two extreme conditions (Sramoon and Sugimoto, 2002; Qin *et al.*, 2004). (1) When the shield machine begins to drive forward, the forces induced by shield machine include: (a) Contact force in point *A* (the segments are just erected, so the contact force is small. the contact force can be set to 0); (b) Forces from tail brush; (c) Jacking forces (Fig.10a); (2) After one driving cycle, jacks draw back. The forces induced by the shield machine include: (a) Contact force in point *C* (since segments have to resist the deviation of shield machine, shield shell applies large forces on segments); (b) The space between tail brush and exterior surfaces of segments decreases, the extrusion forces enlarge (Fig.10b).

The maximum deflection angle of a shield machine is  $\pm 0.3^\circ$  (Zhang *et al.*, 2005). In normal circumstances, the deflection angle can be controlled within  $\pm 0.1^\circ$ . Therefore, in this paper, in order to reflect the general situation, the deflection angle was assumed to be  $\pm 0.1^\circ$ . Horizontal direction is assumed to be *X* axis. Vertical direction is assumed to be *Y* axis. Driving direction of shield machine is assumed to be *Z* axis. The irregular motion attitude of shield machine can be simplified to four deflection model: (1) Dev 1: rotate  $0.1^\circ$  about positive direction of *Y* axis (Fig.11b); (2) Dev 2: rotate  $0.1^\circ$  about negative direction of *Y* axis (Fig.11c); (3) Dev 3: rotate  $0.1^\circ$  about positive direction of *X* axis (Fig.11d); (4) Dev 4: rotate  $0.1^\circ$  about negative direction of *X* axis (Fig.11e).

Squeezing action induced by a shield machine can be modeled as the contact interaction between tail brush and segments. Contact surfaces were set between the inner surfaces of tail brush and segment exterior surfaces (Fig.12). When the shield machine drives with deflection, the contact forces, including normal force and sliding-frictional force are automatically computed by ADINA program through iterative process. Thus the contact interaction can simulate squeezing action. The friction coefficient of tail brush and segment is set to 0.3.

Based on discussions from subsection "Jacking forces" to subsection "Squeezing action induced by shield machine", the load distribution along driving direction is summed up as Fig.13.

When a driving cycle begins, R1 erection has just been completed, and the shield machine tail

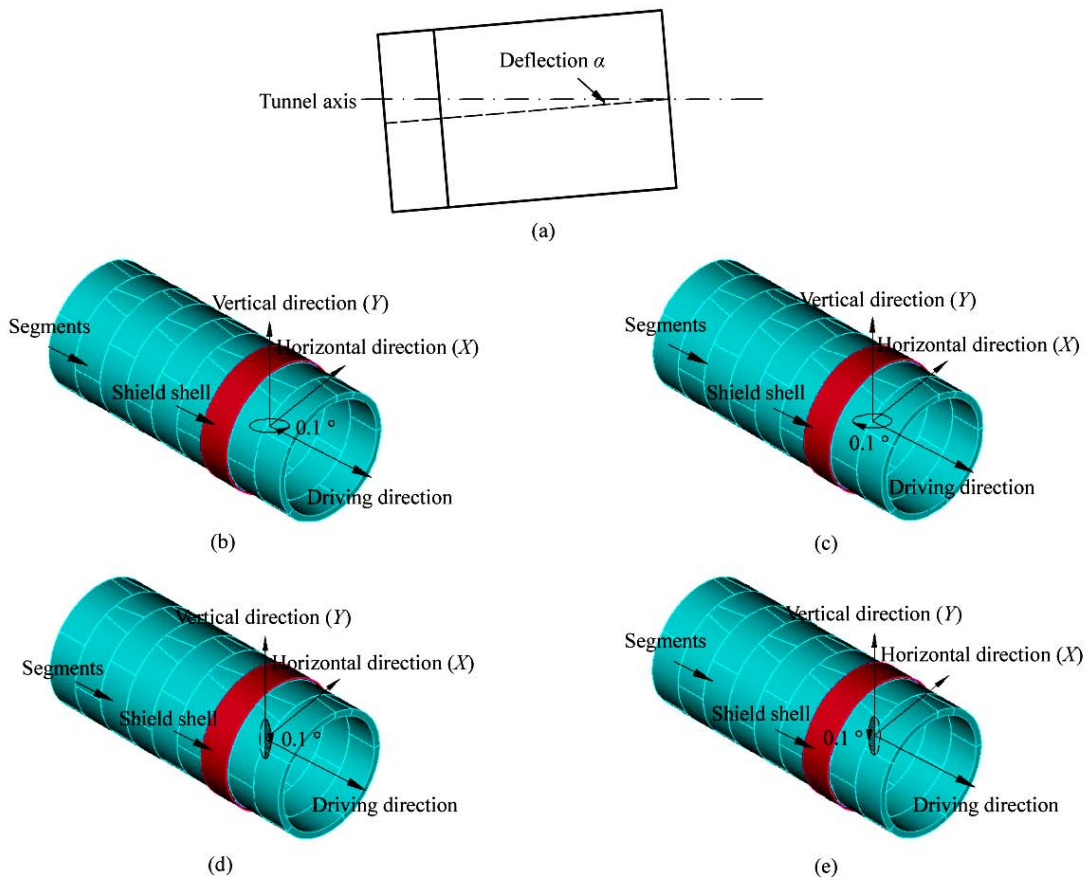


Fig.11 Driving attitude of shield machine. (a) Abstract model; (b) Dev 1; (c) Dev 2; (d) Dev 3; (e) Dev 4

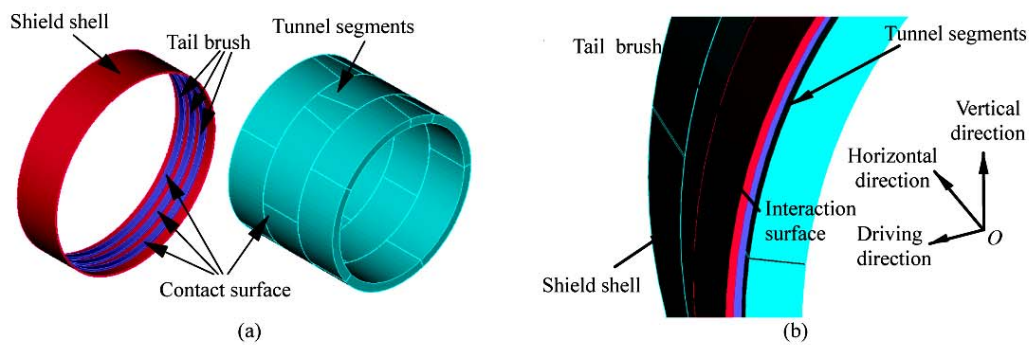


Fig.12 Interaction between tail brush and segments. (a) Contact surfaces between tail brush and tunnel segments; (b) 3D position relation of contact surfaces

locates on R3. Then the shield machine drives forward and stops at R2 and, the jacks draw back. A driving cycle completes. Fig.13 shows the state when a driving cycle begins. During driving, R1 just bears jacking forces. R2 bears extrusion forces of tail brush. R3 gradually leaves the shield machine and bears increasing grouting pressure. The grouting pressure

gradually reaches  $P_{in1}$  and  $P_{in2}$ . Grouting materials surrounding R4~R7 gradually solidify. Hence, in this paper, for R4~R7, it was assumed that grouting pressure linearly decreases from  $P_{in1}$  to  $P_{in2}$  and then from  $P_{in2}$  to  $P_2$  (Fig.4). For R8 and R9, it was assumed that the grouting materials have been concretionary, and the earth pressure directly acted on exterior sur-

faces of R8 and R9 (Zhang *et al.*, 2005) (Fig.4). Generally, the load-structure theory and the load distribution in this paper are approximate to practical situation, and these two methods are adequate to the main research aspect of this paper. Only the elaborate ground-structure method (Kasper and Meschke, 2004) can account for the complex interactions at the construction stage.

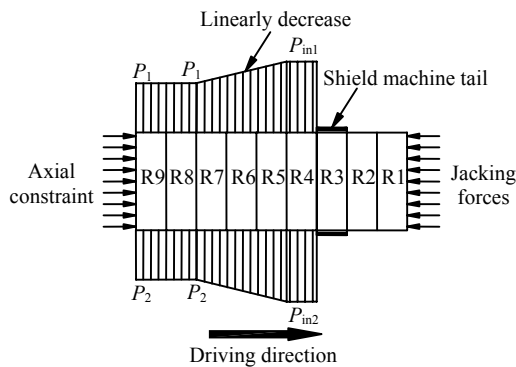


Fig.13 Loads distribution along longitudinal direction

FINITE ELEMENT MODEL

Dimensions of segment and shield machine tail

The segment arrangement and numbering are showed in Figs.14 and 15. The segment dimensions are displayed in Fig.15. Segment external diameter is 6 m; internal diameter is 5.4 m; width is 1.5 m; and thickness is 0.3 m (Figs.14 and 15). A segment ring consists of one key segment (KP), two adjacent segments (BP and CP) and three standard segments (A1P~A3P). The key segment deviates 18° from vertical direction (Figs.14 and 16). The tunnel structure is erected by staggered format (Fig.16). Internal diameter of tail brush is 5.99 m. Internal diameter of shield shell is 6.13 m. Thickness of shield shell is 40 mm.

Material model and main parameters

Material models used in the numerical model are listed in Table 1.

In common computation, Young’s modulus of steel is  $2.06 \times 10^8$  kPa. However, in Table 1, Young’s modulus of M24 steel bolts is  $5.4 \times 10^7$  kPa. In this paper, straight bolt was applied to simulate curved bolt. Obviously, stiffness of straight bolt is larger than that of curved bolt when bearing tensile force.

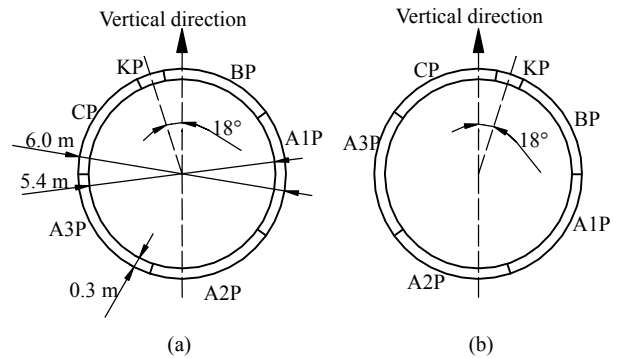


Fig.14 (a) Segment arrangement and (b) relative numbering. KP, BP and A1P~A3P denote segment number

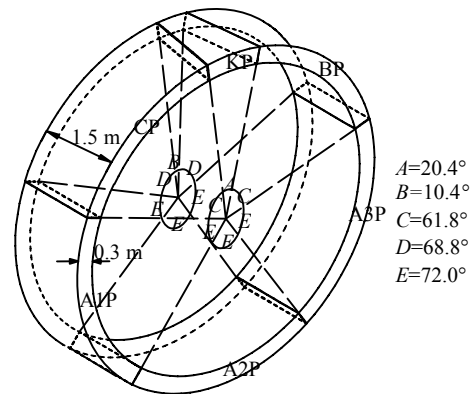


Fig.15 Segment dimensions. A to E denote segment central angle

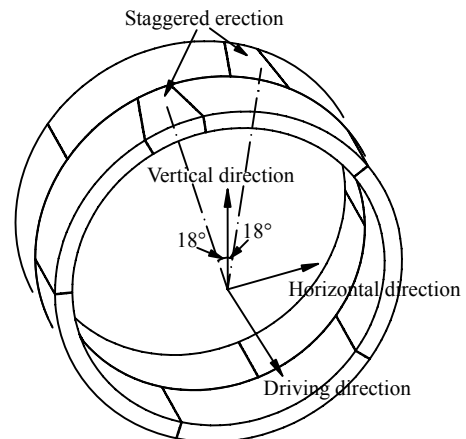


Fig.16 Staggered erection. 18° is staggered angle used in Guangzhou Metro

If Young’s modulus of straight bolt is unchanged, the stiffness would be larger than practical situation. Hence, in order to obtain the equivalent Young’s modulus of straight bolt, the same tensile force was applied to the straight bolt and curved bolt. Through adjusting the Young’s modulus of straight bolt, the

displacement of straight bolt is the same as that with curved bolt, and the Young's modulus of straight bolt is  $5.4 \times 10^7$  kPa. Grouting material can flow down after being injected into gaps between tunnel segments and soil stratum. The grouting material can fill the voids of lower part of tail brush. Therefore, for the same tail brush, Young's modulus of lower part is larger than that of upper part (Table 1).

### 3D FE model

The numerical model consists of nine segment rings. The whole model, including segments, bolts, sealing rods, pads, shield shell, tail brush and soil stratum, were meshed by 8-node 3D solid element. When creating an input file for computational solver, ADINA preprocessing program automatically uses 3D truss elements to mesh the lines, which are designated as rebar elements. Simultaneously, for each rebar line, the ADINA preprocessing program finds

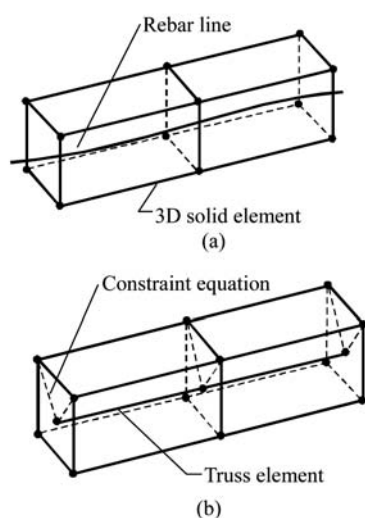


Fig.17 Rebar in 3D solid element of ADINA model. (a) Status before creating input file; (b) Status after creating input file

the intersections of rebar line and the faces of 3D solid elements. Then the preprocessing program generates nodes at these intersections and generates truss elements that connect the successive nodes. The preprocessing program also defines constraint equations between the generated nodes and three corner nodes of the 3D solid element faces (ADINA R&D Inc., 2005). Fig.17 shows the changes of rebar elements before and after creating ADINA input file.

Contact function was applied to simulate the interaction of each sealing rod (friction coefficient is 0.1). Squeezing action induced by shield machine and ground reaction was also simulated with contact function (subsections "Ground reaction" and "Squeezing action induced by shield machine"). Each segment is jointed by M24 straight bolts. Initial strain was added to bolt elements to simulate the pretightening twist moment of 300 N·m.

The numerical model included 60600 elements and 93266 nodes (Fig.18). The horizontal direction is  $X$  axis, the vertical direction is  $Y$  axis, and the driving direction of shield machine is assumed to be  $Z$  axis.

## RESULTS AND ANALYSIS

The present paper focuses on rebar stress, so the descriptions and analysis only related to the rebar stress which would be shown in the following parts. The segment displacement, stress and strain are neglected. The positive value represents tension stress, while the negative value represents compression stress.

### Normal construction status

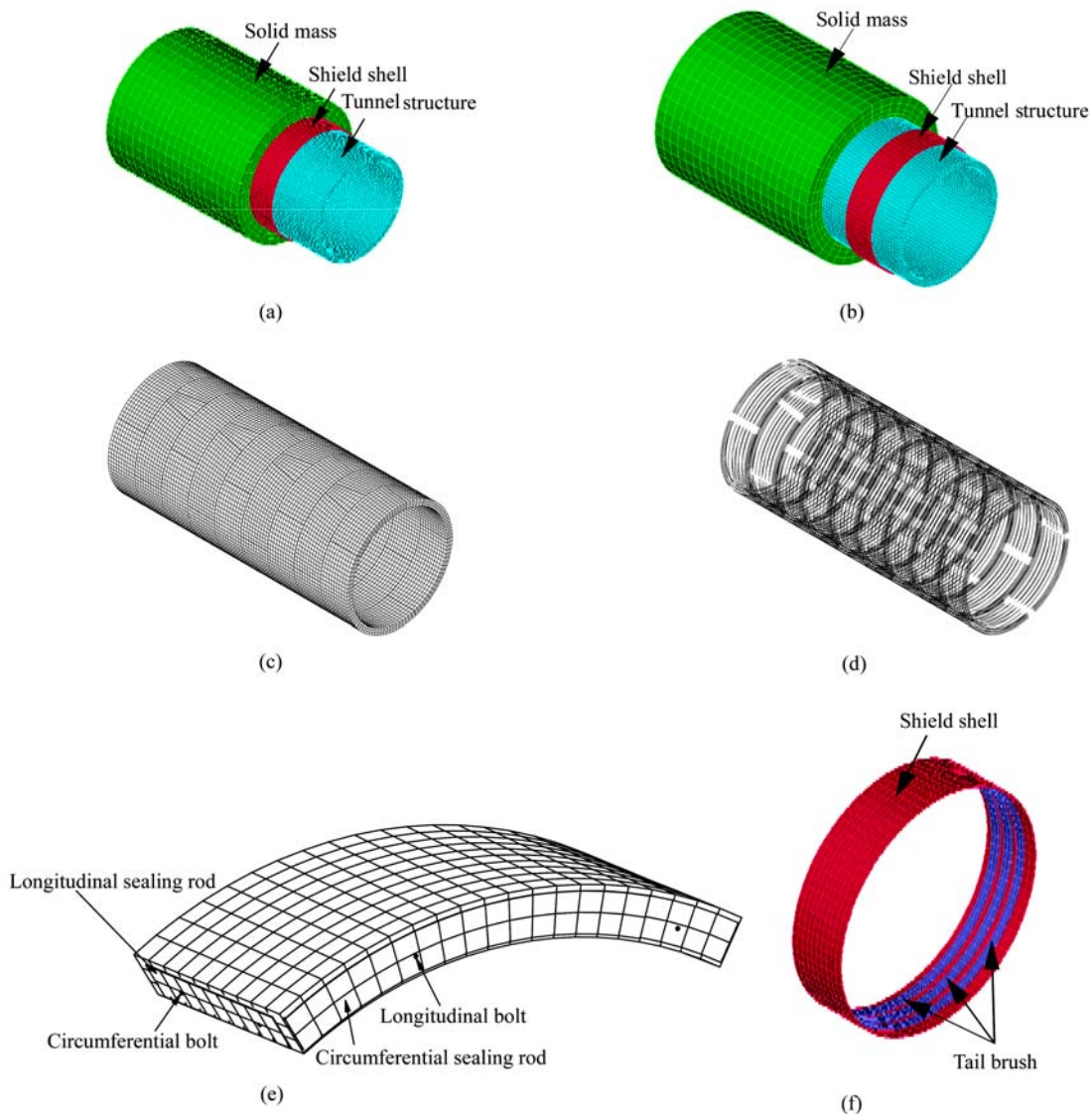
Stress distribution of rebar is showed in Fig.19. The peak values of rebar stress of R1 to R9 are showed in Fig.20. Compressions  $A$  and  $B$  denote

Table 1 Material models and parameters

Type	Material	Constitutive model	Material parameter
Segment	Concrete	Elasticity	$E=3.45 \times 10^7$ kPa, $\nu=0.2$ , $\gamma=25$ kN/m <sup>3</sup>
Rebar	Steel	Elasticity	$E=5.4 \times 10^7$ kPa, $\nu=0.167$
M24 Bolt	Steel	Elasticity	$E=5.4 \times 10^7$ kPa, $\nu=0.167$
Sealing rod cork gasket	Rubber	Mooney-Rivlin	$C_1=561$ kPa, $C_2=225$ kPa
Shield shell	Steel	Elasticity	$E=2.06 \times 10^8$ kPa, $\nu=0.167$
Tail brush (upper part)	—	Elasticity	$E=4.0 \times 10^4$ kPa, $\nu=0.2$
Tail brush (lower part)	—	Elasticity	$E=3.45 \times 10^5$ kPa, $\nu=0.2$
Solid mass	—	Elasticity	$E=2.0 \times 10^4$ kPa, $\nu=0.3$

$E$  is Young's modulus;  $\nu$  is Poisson's ratio;  $\gamma$  is volume weight;  $C_1$  and  $C_2$  are parameters of Mooney-Rivlin model





**Fig.18** Finite element mesh of numerical model. (a) Whole model (before driving cycle); (b) Whole model (after driving cycle); (c) Tunnel model; (d) Rebar elements of whole tunnel; (e) Bolts and sealing rods; (f) Shield tail

compression stresses after and before jacking apparatus moves backward, respectively; Tensions *A* and *B* denote tension stresses after and before jacking apparatus moves backward, respectively.

Fig.19 indicates that tension stress only appears in R1, R2, R8 and R9. Comparison of the rebar stresses before and after jacking apparatus moves backward shows that jacking forces cause rebar in R1 and R2 to bear tension force. After jacking apparatus moves backward, the rebar stress of R2 becomes compressive stress. The peak values in Fig.20a indicate that the maximum values of compression and

tension stresses are 21.2% and 6.0% of the rebar design strength, respectively. The general stress level is lower.

The peak stresses of R1~R2 indicate that the jacking forces just affect R1 and R2. R1 just bears jacking forces, thereby the tension stress ratio before and after jacking apparatus moves backward reaches 11.8 and the relevant compression stress ratio reaches 17.9. R3 to R7 bear grouting pressure and the effects of jacking forces on R3 to R7 gradually weakened. For R3~R7, the tension stress ratio before and after jacking apparatus moves backward is between 1.04

and 1.23, and the relevant compression stress ratio is between 1.06 and 1.1. The stress range is  $-65$  MPa to  $20$  MPa. The general stress level is lower. The rebar is in elastic status.

The rebar stress measured in Guangzhou Metro is showed in Fig.20b (Chen *et al.*, 2004). The number, such as  $73^\#$ , represents the monitoring point inside segment. The computation results of rebar stress approach the actual measurement results.

### Driving attitude of shield machine with deviation

Due to the similarity of stress distribution of shield machine model with an inclination (Dev model), this section just presents the rebar stress of Dev 1 (Fig.21). The peak values of rebar stress of all Dev model are showed in Fig.22. In Fig.22, Dev 1 Tension *B* denotes the tension stress of model Dev 1 before jacking apparatus moves backward. Dev 1 Compression *A* denotes the compression stress of

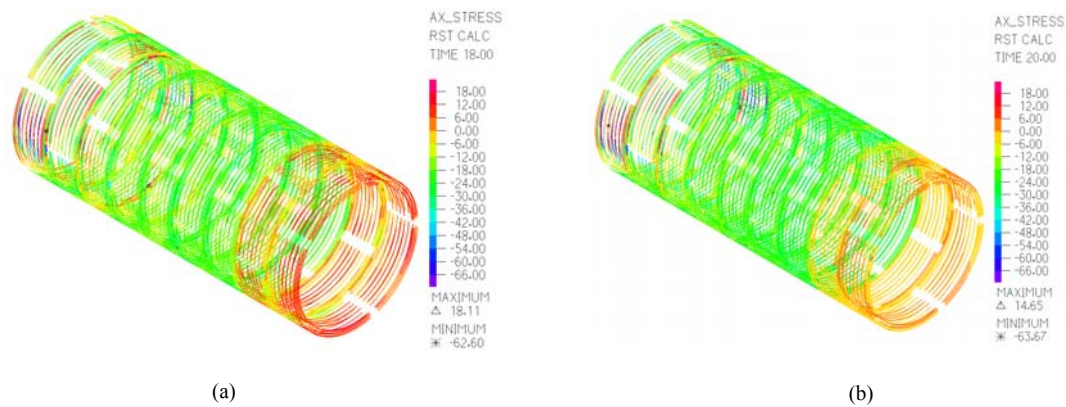


Fig.19 Stress distribution of rebar in normal construction status (MPa). Stress before (a) and after (b) jacking apparatus moves backward

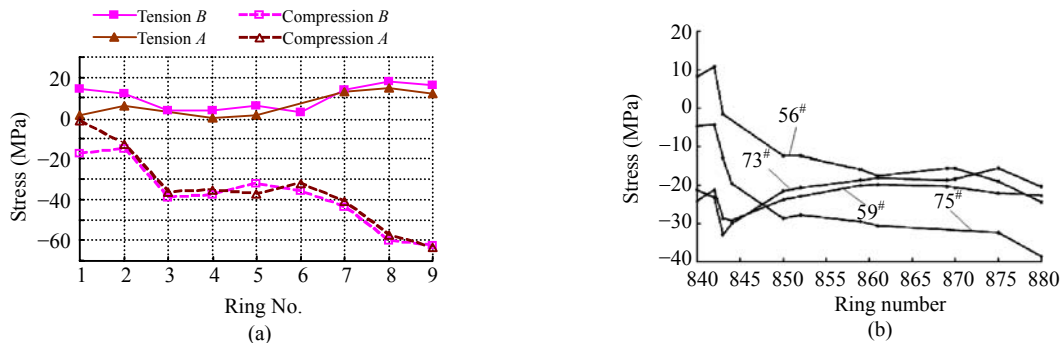


Fig.20 Peak value of rebar stress in normal construction status. (a) Results of this paper; (b) Actual measurement results of Guangzhou Metro

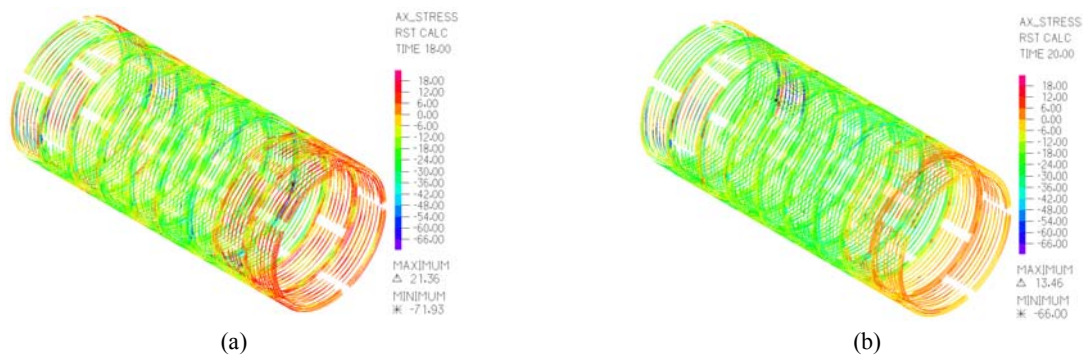


Fig.21 Stress distribution of rebar in Dev 1 (MPa). Stress before (a) and after (b) jacking apparatus moves backward

model Dev 1 after jacking apparatus moves backward. Other symbols use the same rule. The differential values (DV) compared to the results of normal construction status are showed in Fig.23. The values of Fig.23 are the differential values which are the results of Dev model subtract the results of normal construction status. Therefore, for tension stress, the larger positive value deviates the normal construction status further. For compression stress, the lesser negative value deviates the normal construction status further.

Figs.20 to 23 indicate that the deviation of shield machine attitude apparently influences rebar stress, especially rebar stress of R1~R7 before jacking apparatus moves backward. In Dev model, influence of jacking force expands to R4. Tension stress appears in R1 to R4, R8 and R9.

Before the jacking apparatus moves backward, the maximum amplitude of compression stress is

71.93 MPa which is twice of that in the normal construction status and the maximum amplitude of tension stress is 42.95 MPa which is three times of that in the normal construction status. Fig.22 indicates that the influence range of jacking forces expands from R1~R2 to R1~R4. When the driving attitude of a shield machine deviates, the action direction of jacking forces that R1 bears is not along the tunnel axis which further enlarges the differential values. For R1~R2, the tension stress ratio before and after jacking apparatus moves backward reaches 34.9, and the relevant compression stress ratio reaches 34.9. For R3~R7, the tension stress ratio before and after jacking apparatus moves backward is between 1.0 and 9.6, and the relevant compression stress ratio is between 1.0 and 1.5. The stress range is -80 MPa to 50 MPa. The general stress level is lower. The rebar is in elastic status. The results of rebar stress approach actual measurement results (Chen et al., 2004).

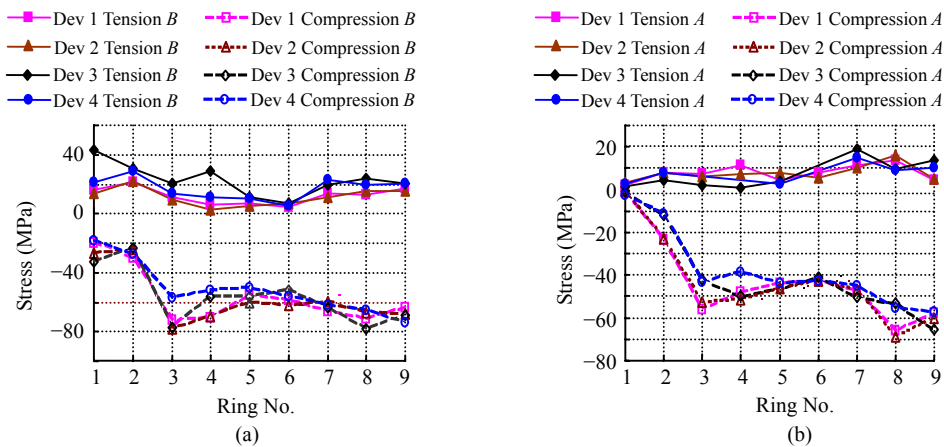


Fig.22 Peak value of rebar stress in deflection status. Stress before (a) and after (b) jacking apparatus moves backward

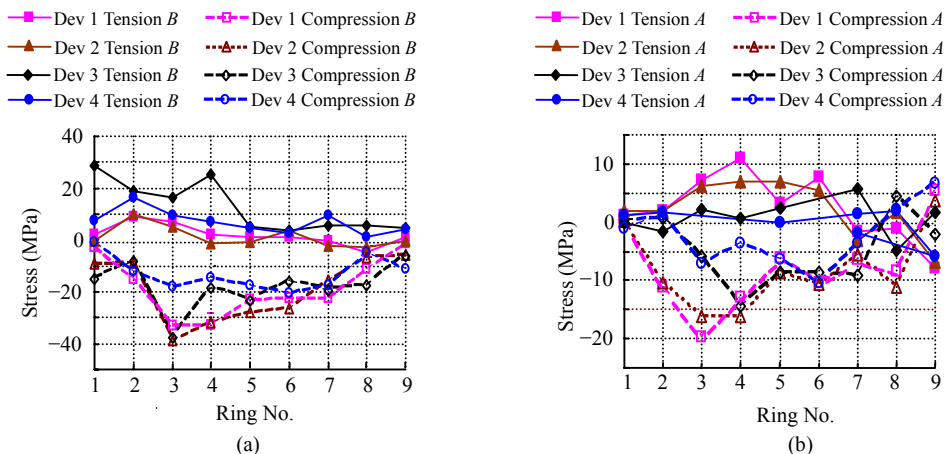


Fig.23 Differences between rebar stress compare to normal construction status. Stress before (a) and after (b) jacking apparatus moves backward

## CONCLUSION

Through analyzing rebar stress of a 3D shield tunnel numerical model with 9 rings, some conclusions are drawn as follows:

(1) In normal construction status, the rebar of segment is in elastic status and its stress is between  $-65$  MPa and  $20$  MPa.

(2) When shield machine drives with deviation, the stress of segment rebar is between  $-80$  MPa and  $50$  MPa, and the rebar is in elastic status. Driving attitude of shield machine has effect on rebar stress distribution and peak value. Comparison of the rebar stress before and after the jacking apparatus moves backward shows that the stress increment after jacking apparatus moves backward is between  $0$  and  $20$  MPa. In general, the rebar is in elastic status.

(3) The stress of segment rebar is at a low level, which accords with actual measurement. Even as some cracks appear on segments, the stress of segment rebar is still at a low level. That is to say, the segment rebar cannot protect the plain concrete covering layer of segment. Certain impact force or tension stress causes the crack of the thick plain concrete covering layer. It is helpful to incorporate a certain quantity of steel fiber to improve the anti-crack and shock resistance performance.

## References

- ADINA R&D Inc., 2005. Theory and Modeling Guide Volume I: ADINA Solids & Structures. Watertown, MA.
- Blom, C.B.M., Horst, E.J.V., Jovanovic, P.S., 1999. Three-dimensional structural analyses of the shield-driven "Green Heart" tunnel of the high-speed line south. *Tunnelling and Underground Space Technology*, **14**(2):217-224. [doi:10.1016/S0886-7798(99)00035-8]
- Chen, W., Peng, Z.B., Tang, M.X., 2004. Testing study on working property of shield segment. *Chinese Journal of Rock Mechanics and Engineering*, **23**(6):959-963 (in Chinese).
- Dobashi, H., Kawada, N., Shiratori, A., 2004. A rational design of steel segmental lining in large dimensional shield tunnels for rapid post-excavation method. *Tunnelling and Underground Space Technology*, **19**(4-5):457-458. [doi:10.1016/j.tust.2004.02.065]
- Kasper, T., Meschke, G., 2004. A 3D finite element simulation model for TBM tunnelling in soft ground. *International Journal for Numerical and Analytical Methods in Geomechanics*, **28**(14):1441-1460. [doi:10.1002/nag.395]
- Koyama, Y., 2003. Present status and technology of shield tunneling method in Japan. *Tunnelling and Underground Space Technology*, **18**(2-3):145-149. [doi:10.1016/S0886-7798(03)00040-3]
- Li, H.P., An, H.W., Xia, M.Y., 2006. Analysis of dynamic character of tunneling shield machine. *Chinese Journal of Underground Space and Engineering*, **2**(1):101-103 (in Chinese).
- Li, Z.N., 2001. Discussion on Manufacture Tolerance of Shield Tunnel Segment. Papers of 14th Meeting of Council of Fast Track Communication of China Civil Engineering Society, Beijing, p.308-312 (in Chinese).
- Li, Z.N., Chen, L.N., 2003. Discussion on Form of Reinforcement in Segment of Shield Tunnel. Papers of 15th Meeting of Council of Fast Track Communication of China Civil Engineering Society, Chengdu, p.73-75 (in Chinese).
- Mashimo, H., Ishimura, T., 2003. Evaluation of the load on shield tunnel lining in gravel. *Tunnelling and Underground Space Technology*, **18**(2-3):233-241. [doi:10.1016/S0886-7798(03)00032-4]
- Nomoto, T., Imamura, S., Hagiwara, T., Kusakabe, O., Fujii, N., 1999. Shield tunnel construction in centrifuge. *Journal of Geotechnical and Geoenvironmental Engineering*, **125**(4):289-300. [doi:10.1061/(ASCE)1090-0241(1999)125:4(289)]
- Qin, J.S., Zhu, W., Chen, J., 2004. Study of dislocation of duct pieces and crack problems caused by shield attitude control. *Construction Technology*, **33**(10):25-27 (in Chinese).
- Sramoon, A., Sugimoto, M., 2002. Theoretical model of shield behavior during excavation. *Journal of Geotechnical and Geoenvironmental Engineering*, (2):138-165.
- Terzaghi, K., Peck, R., Mesri, G., 1996. Soil Mechanics in Engineering Practice. John Wiley and Sons, New York, p.104-105.
- Working Group No.2, International Tunneling Association, 2000. Guidelines for the design of shield tunnel lining. *Tunnelling and Underground Space Technology*, **15**(3):303-331. [doi:10.1016/S0886-7798(00)00058-4]
- Zhang, H.B., Yin, Z.Z., Zhu, J.G., Li, C.X., 2005. Three-dimensional FEM simulation of shield-driven tunneling during construction stage. *Rock and Soil Mechanics*, **26**(6):990-994 (in Chinese).
- Zhang, H.M., Guo, C., Fu, D.M., 2002. Study on load test of segment joint in shield driven tunnel. *Modern Tunneling Technology*, **39**(6):28-33 (in Chinese).
- Zhu, W.B., Ju, S.J., 2003. Causes and countermeasures for segment cracking in shield-driven tunnel. *Modern Tunneling Technology*, **40**(1):21-25 (in Chinese).